

# How uncertainties in future climate change predictions translate into future terrestrial carbon fluxes

MARIE BERTHELOT<sup>\*1</sup>, PIERRE FRIEDLINGSTEIN<sup>\*</sup>, PHILIPPE CIAIS<sup>\*</sup>,  
JEAN-LOUIS DUFRESNE<sup>†</sup> and PATRICK MONFRAY<sup>‡</sup>

<sup>\*</sup>Institut Pierre-Simon Laplace, Laboratoire des Sciences du Climat et de l'Environnement, Commissariat à l'Energie Atomique, l'Orme des Merisiers, 91191 Gif sur Yvette, France, <sup>†</sup>Institut Pierre-Simon Laplace, Laboratoire de Météorologie Dynamique, Université Paris 6, 4 place Jussieu, 75252 Paris, France, <sup>‡</sup>Laboratoire d'Etudes en Géophysique et Océanographie Spatiale, 18 avenue Edouard Belin, 31401 Toulouse Cedex 4, France

## Abstract

We forced a global terrestrial carbon cycle model by climate fields of 14 ocean and atmosphere general circulation models (OAGCMs) to simulate the response of terrestrial carbon pools and fluxes to climate change over the next century. These models participated in the second phase of the Coupled Model Intercomparison Project (CMIP2), where a 1% per year increase of atmospheric CO<sub>2</sub> was prescribed. We obtain a reduction in net land uptake because of climate change ranging between 1.4 and 5.7 Gt Cyr<sup>-1</sup> at the time of atmospheric CO<sub>2</sub> doubling. Such a reduction in terrestrial carbon sinks is largely dominated by the response of tropical ecosystems, where soil water stress occurs. The uncertainty in the simulated land carbon cycle response is the consequence of discrepancies in land temperature and precipitation changes simulated by the OAGCMs. We use a statistical approach to assess the coherence of the land carbon fluxes response to climate change. The biospheric carbon fluxes and pools changes have a coherent response in the tropics, in the Mediterranean region and in high latitudes of the Northern Hemisphere. This is because of a good coherence of soil water content change in the first two regions and of temperature change in the high latitudes of the Northern Hemisphere.

Then we evaluate the carbon uptake uncertainties to the assumptions on plant productivity sensitivity to atmospheric CO<sub>2</sub> and on decomposition rate sensitivity to temperature. We show that these uncertainties are on the same order of magnitude than the uncertainty because of climate change. Finally, we find that the OAGCMs having the largest climate sensitivities to CO<sub>2</sub> are the ones with the largest soil drying in the tropics, and therefore with the largest reduction of carbon uptake.

*Keywords:* climate change, CO<sub>2</sub>, terrestrial carbon cycle

*Received 06 October 2003; revised version received 2 November 2004; accepted 14 December 2004*

## Introduction

Our understanding of the impacts of future climate change on the carbon cycle is based on results of climate (ocean and atmosphere general circulation model, OAGCM) and carbon cycle models. A number of former such studies have simulated how the terrestrial carbon uptake increase under rising CO<sub>2</sub>

when making the reasonable assumption that photosynthesis increases with CO<sub>2</sub>, and how this increase is generally reduced when climate change is accounted for. In those studies, carbon cycle models are either forced by climate fields (Cao & Woodward, 1998; Cramer *et al.*, 2001) or directly coupled with OAGCM (Cox *et al.*, 2000; Berthelot *et al.*, 2002; Dufresne *et al.*, 2002). For instance, Cramer *et al.* (2001) used six dynamic global vegetation models, but forced by one scenario of anthropogenic climate to quantify the magnitude of the terrestrial ecosystems response to climate change. They found that the land carbon uptake is reduced by about 50% because of future climate

Correspondence: Marie Berthelot, tel +33 1 55 07 85 75, fax +33 1 55 07 85 79, e-mail: mb@climipact.com

<sup>1</sup>Present address: CLIMPACT, 12 Rue de Belzunce, 75010, Paris, France.

change. By 2100, the land uptake ranges between 3.7 and 8.6 GtC yr<sup>-1</sup> under CO<sub>2</sub> change only, and ranges only between 0.3 and 6.6 GtC yr<sup>-1</sup> when climate change is also accounted for. However, such an analysis does not account for the uncertainty because of the future climate as simulated by the AOGCMs. Results from intercomparison projects, such as the Coupled Model Intercomparison Projects CMIP1 and CMIP2, clearly show that there is also a large uncertainty in the simulated climate (Meehl *et al.*, 2000; Covey *et al.*, 2003). For example, the CMIP2 highlights an increase in global temperature between 1.1 °C and 3.1 °C at the time of CO<sub>2</sub> doubling and a percentage change of the global mean precipitation (PPT) ranging from -0.2% to +5.6% (IPCC 2001).

Hereafter, a conceptually static land carbon cycle model, SLAVE (Friedlingstein *et al.*, 1995), is driven by different scenarios of climate change produced in the context of CMIP2 (Meehl *et al.*, 2000; Covey *et al.*, 2003). Our objective is to examine how uncertainties in future climate change predictions translate into uncertainties in future carbon fluxes. We first describe the terrestrial carbon model and the input climate scenarios. We then calculate how much those changing climates impact the terrestrial uptake of carbon. The mechanisms by which different climate scenarios may regionally increase or decrease carbon sinks are analyzed, as well as the robustness of those results to the different climate scenarios and to changing parameters of the carbon models, the effect of CO<sub>2</sub> increase on net primary productivity (NPP) and the temperature dependency of soil respiration. We suggest that there is a relationship between the sensitivity of the land carbon uptake to temperature increase and the sensitivity of temperature increase to an increase in atmospheric CO<sub>2</sub>.

## Carbon cycle model and climate scenarios

### *The terrestrial carbon cycle model*

The carbon model, called SLAVE, accounts for nine natural ecosystems and croplands (Friedlingstein *et al.*, 1995; Friedlingstein *et al.*, 1999), whose distribution is held to be constant during all the periods of simulation. The land cover is based on data set observations from Matthews (1983). Terrestrial carbon cycling is driven by the GCM monthly fields of surface temperature, PPT, solar radiation and by the annual atmospheric CO<sub>2</sub> concentration, which directly influences NPP. The model computes the water budget, NPP, allocation, phenology, biomass, litter and soil carbon budgets. Carbon assimilated through NPP is allocated to three phytomass pools: leaves, stems and roots. Litter and soil carbon pools are both divided into metabolic and

structural components. NPP is a function of the three climatic variables following a light use efficiency formulation, where light use efficiency is sensitive to temperature and PPT (Potter *et al.*, 1993):

$$\text{NPP}_0 = \varepsilon \times \text{APAR} \times T_{\varepsilon 1} \times T_{\varepsilon 2} \times W_{\varepsilon}. \quad (1)$$

The absorbed photosynthetically active radiation (APAR) is deduced from incoming solar radiation and from Leaf Area Index (LAI) (Sellers *et al.*, 1996), LAI being diagnosed from the calculated leaf biomass.  $\varepsilon$  is the maximum light use efficiency. The first temperature stress factor,  $T_{\varepsilon 1}$ , which depresses NPP at very high and low temperatures, varies from 0.8 at 0 °C to 1.0 at 20 °C to 0.8 at 40 °C and is set equal to zero for monthly temperatures below -10 °C (Potter *et al.*, 1993). The second temperature stress factor,  $T_{\varepsilon 2}$ , depresses NPP when the temperature is above or below the optimum temperature (defined as the air temperature in the month when the NDVI reaches its maximum for the year (Los *et al.*, 1994)), the reduction being greater at high than at low temperatures (Potter *et al.*, 1993). The soil water stress term,  $W_{\varepsilon}$ , is a function of evapotranspiration and varies from 0 in very dry ecosystems to 1 in very wet ecosystems.

The soil water content (SWC) is computed as the balance between monthly precipitation (PPT) and actual evapotranspiration (AET). AET is limited by the potential evapotranspiration (PET) and by the available water (PPT + extractable soil water). PET is calculated following Thornthwaite formulation (Thornthwaite, 1948; Thornthwaite & Mather, 1957). We note the Thornthwaite formulation only uses temperature, and is not based on an energy budget. There are now more suitable methods to estimate PET, such as Penman-Monteith or Priestly-Taylor, but the Thornthwaite approach is the only one that we could use with the climate data time-series available from the CMIP2 project, which are monthly surface temperature and monthly PPT.

The SWC, as simulated by SLAVE, is the water quantity in the first 30 cm of soil but is limited by an upper limit ( $Q_{\text{max}}$ ).

The NPP increases in response to increasing CO<sub>2</sub> (Wullschlegel *et al.*, 1995; DeLucia *et al.*, 1999) under a Michaelis-Menten  $\beta$  factor formulation (Gifford, 1992).  $\beta$  is a function of SWC ( $f_{\text{SWC}}$ ), nitrogen ( $f_{\text{N}}$ ) and phosphorus ( $f_{\text{P}}$ ) availabilities (Friedlingstein *et al.*, 1995):

$$\beta = \beta_0 f_{\text{SWC}} f_{\text{N}} f_{\text{P}}. \quad (2)$$

For each litter and soil carbon pools, heterotrophic respiration (RH) is calculated as the product of the pool carbon content ( $C_i$ ) by a decomposition rate depending

**Table 1** Climate models used to simulate the impact of climate changes on terrestrial carbon cycling

OAGCM	Origin	Initial atmospheric CO <sub>2</sub>
BMRC	<i>Bureau of Meteorological Research, Australia</i>	330
CCCMA	<i>Climate Center, Canada</i>	330
CCSR	<i>Center for Climate System Research, Japan</i>	345
CERFACS	<i>Centre Européen de Recherche et de Formation Avancée en Calcul Scientifique, France</i>	353
CSIRO	<i>Commonwealth Scientific and Industrial Research Organisation, Australia</i>	330
DOE	<i>Department of Energy Parallel Climate Model, USA</i>	355
ECHAM3	<i>Max Planck Institute for Meteorology, Germany</i>	345
GFDL	<i>Geophysical Fluid Dynamics Laboratory, USA</i>	360
GISS	<i>Goddard Institute for Space Sciences, USA</i>	315
IAP	<i>Institute for Atmospheric Physics, China</i>	345
IPSL	<i>Institut Pierre Simon Laplace, France</i>	320
MRI	<i>Meteorological Research Institute, Japan</i>	345
NCAR	<i>National Center for Atmospheric Research, USA</i>	355
UKMO	<i>United Kingdom Meteorological Office, Great Britain</i>	290

OAGCM, ocean-atmosphere general circulation model.

on soil moisture and temperature:

$$RH = \sum_{i=1}^4 K_i \times C_i, \quad (3)$$

where

$$K_i = K_{i,\max} \times f_T \times f_{H_2O}. \quad (4)$$

The optimal decomposition rate  $K_{i,\max}$  equals 10.4 yr<sup>-1</sup> for metabolic litter, 0.58 yr<sup>-1</sup> for structural litter and 0.006 yr<sup>-1</sup> for decomposing soil organic matter (at 30 °C). The temperature sensitivity function,  $f_T$ , is a  $Q_{10}$  function: a temperature increase of 10 °C induces an increase of a factor of  $Q_{10}$  of the decomposition rate, with  $Q_{10}$  being fixed to 2 for each pool. The SWC dependency,  $f_{H_2O}$ , first increases when SWC increases, saturates under optimal humidity conditions and then decreases to account for reduced decomposition under anaerobic conditions (Parton *et al.*, 1993).

### Methods

We used the output of coupled ocean-atmosphere general circulation models (OAGCM), listed in Table 1, which participated in the CMIP2. We selected 14 among the 20 original models, keeping only the most recent version of each model when several were available, and discarding simulations shorter than 80 years. These are BMRC (Power *et al.*, 1998; Colman, 2001), CCCMA (Boer *et al.*, 2000; Flato *et al.*, 2000), CCSR (Emori *et al.*, 1999), CERFACS (Barthelet *et al.*, 1998), CSIRO (Gordon & O'Farrell, 1997; Hirst *et al.*, 2000), DOE (Washington *et al.*, 2000), ECHAM3 (Cubasch *et al.*, 1997; Voss *et al.*, 1998), GFDL (Delworth & Knutson, 2000), GISS (Russell *et al.*, 1995; Russell & Rind, 1999), IAP (Wu *et al.*, 1997; Zhang *et al.*, 2000),

IPSL (Khodri *et al.*, 2001), MRI (Tokioka *et al.*, 1996), NCAR (Boville & Gent, 1998) and UKMO (Gordon *et al.*, 2000). The two different CMIP2 simulations consist of a *Control run* with constant greenhouse gas concentrations and of a *Greenhouse run* with increasing CO<sub>2</sub> at a rate of 1% per year. Note that the initial CO<sub>2</sub> mixing ratio depends on the model and varies from 290 to 360 ppmv (Table 1). Both simulations extend for 80 years.

The climate forcing available by the OAGCM of CMIP is monthly or 20 years averaged data. The only monthly surface data available from the CMIP project are surface temperature, PPT and sea level pressure. The other data are not defined at this time step as these were not requested by the CMIP protocol to the OAGCM community. SLAVE was, therefore, ideally suited for the simulations we made, considering the few available monthly variables.

We use the atmospheric CO<sub>2</sub> curve and the OAGCM temperature and PPT to force the land carbon model SLAVE. We do not use soil moisture calculated by OAGCM but compute it in SLAVE as described in the previous section. Two reasons justify this choice: first, this variable is not available at monthly time step in the CMIP data base and, second, most of OAGCM use different soil models (depth, number of layers, soil types, etc.). Therefore, it would not be coherent to force SLAVE with different GCM soil characteristics to compare the impact of soil water change on productivity or RH.

In a first test, we initialized carbon pools and fluxes to equilibrium in SLAVE using the control climate of each OAGCM. This resulted into widely different global NPP estimates, ranging from 32 GtC yr<sup>-1</sup> in BMRC up to 63 GtC yr<sup>-1</sup> in MRI as can be seen in

**Table 2** Net primary production (in Gt C yr<sup>-1</sup>) simulated by SLAVE when forced by the control climate of each OAGCM

OAGCM	NPP (Gt C yr <sup>-1</sup> )
BMRC	32
CCCMA	59
CCSR	45
CERFACS	56
CSIRO	60
DOE	53
ECHAM3	44
GFDL	60
GISS	51
IAP	47
IPSL	50
MRI	63
NCAR	51
UKMO	51
Experiment average	52 ± 8

OAGCM, ocean–atmosphere general circulation model; NPP, net primary productivity.

Table 2. Such discrepancies in the modeled NPP mainly reflect differences in tropical climate among the models. Any combination of temperature and PPT, which implied low SWC in the tropics, always yielded a lower NPP estimate. Thus, in order to cast off the influence of the spread in *control run* climates on the initial state of SLAVE, we decided to initialize SLAVE's carbon pools with an observed climatology constructed from data over the past 150 years (Dai *et al.*, 1997; Hansen *et al.*, 1999) and constant atmospheric CO<sub>2</sub> set to 280 ppmv. From this initial state, we then computed the response of terrestrial carbon pools and fluxes first to rising CO<sub>2</sub> at a rate of 1% yr<sup>-1</sup> without climate change (simulation *Fert* for Fertilization only), and second to rising CO<sub>2</sub> and changing climate according to each OAGCM prediction (simulation *FertClim* for Fertilization plus Climate effects). To ensure continuity between the observed climate fields and those from OAGCM calculations, we used the following equations:

$$\begin{aligned}
 T(t) &= T_0 + \Delta T \\
 \text{with } \Delta T &= T_{\text{GH}} - T_{\text{CON}}, \\
 P(t) &= P_0 + \Delta P \\
 \text{with } \Delta P &= P_0 \frac{(P_{\text{GH}} - P_{\text{CON}})}{P_{\text{CON}}} \quad \text{if } \frac{P_{\text{GH}}}{P_{\text{CON}}} \in [0.5, 2], \\
 \text{and } \Delta P &= (P_{\text{GH}} - P_{\text{CON}}) \quad \text{if } \frac{P_{\text{GH}}}{P_{\text{CON}}} \in [0, 0.5] \\
 &\quad \text{or } [2, +\infty),
 \end{aligned}
 \tag{5}$$

where  $T(t)$  and  $P(t)$  are the perturbed temperature and PPT used in the *FertClim* case, and  $T_0$  and  $P_0$  their

climatological values; the GH (respectively, CON) subscript refer to the greenhouse run (respectively, control run) of each OAGCM. The use of two arbitrary thresholds in the computation of  $P(t)$  allows us to filter out unrealistic PPT values when the ratio  $P_{\text{GHR}}/P_{\text{CON}}$  is either too large or too small. As changes in incoming short-wave radiation have small impacts on NPP in SLAVE (Berthelot *et al.*, 2002), we maintained this forcing constant (Bishop & Rossov, 1991) in both *Fert* and *FertClim* simulations.

#### Short description of the different simulated climate

We describe here the changes in land temperature and PPT deduced from Eqn (5) as well as those of SWC as calculated into SLAVE. This is a necessary first step to further understand in the following how climate will impact the modeled land uptake of CO<sub>2</sub>.

Regarding temperature, we focus here on three models, UKMO, DOE and IAP, that are illustrative of the range in land temperature change as shown in Fig. 1a and b. We picked up UKMO as the warmest model over continents (+3.5 °C at 2CO<sub>2</sub>) and DOE as the coldest one (+2 °C at 2CO<sub>2</sub>). UKMO is also the warmest model at any latitude, whereas DOE is globally the coldest but yet shows a significant warming at northern latitudes (Fig. 1b). In both UKMO and DOE, the warming over land is more pronounced at northern latitudes than in the tropics, which is not the case in IAP (Fig. 1b). Regarding PPT, there are very large spatial differences between the 14 models (Fig. 1c and d). In global rainfall, the wettest models are CERFACS and IAP with an 8% increase, and the driest one is CCCMA with a 2% decrease. Such large model spread for PPT primarily reflects discrepancies in the tropics of up to 650 mm yr<sup>-1</sup> between the two extreme models (IAP and CCCMA), while on the other hand, all models robustly predict an increase in PPT at high northern latitudes (Fig. 1d). SWC, critical in calculating biospheric fluxes within SLAVE, depends on PPT and temperature through evapotranspiration. Maximum decrease in global SWC is found in the warmest UKMO (-15%) and in the driest CCCMA simulations (-12%) (Fig. 1e). Note that, generally, a global decrease in SWC reflects mostly a drying of tropical soils, whereas in the Northern Hemisphere SWC can even increase (Fig. 1f).

#### Impact on terrestrial carbon fluxes

##### *Spatial patterns in the response of carbon uptake to climate change*

Net ecosystem production (NEP) calculated from the difference between NPP and RH would be an increasing sink with time in the absence of climate change, but

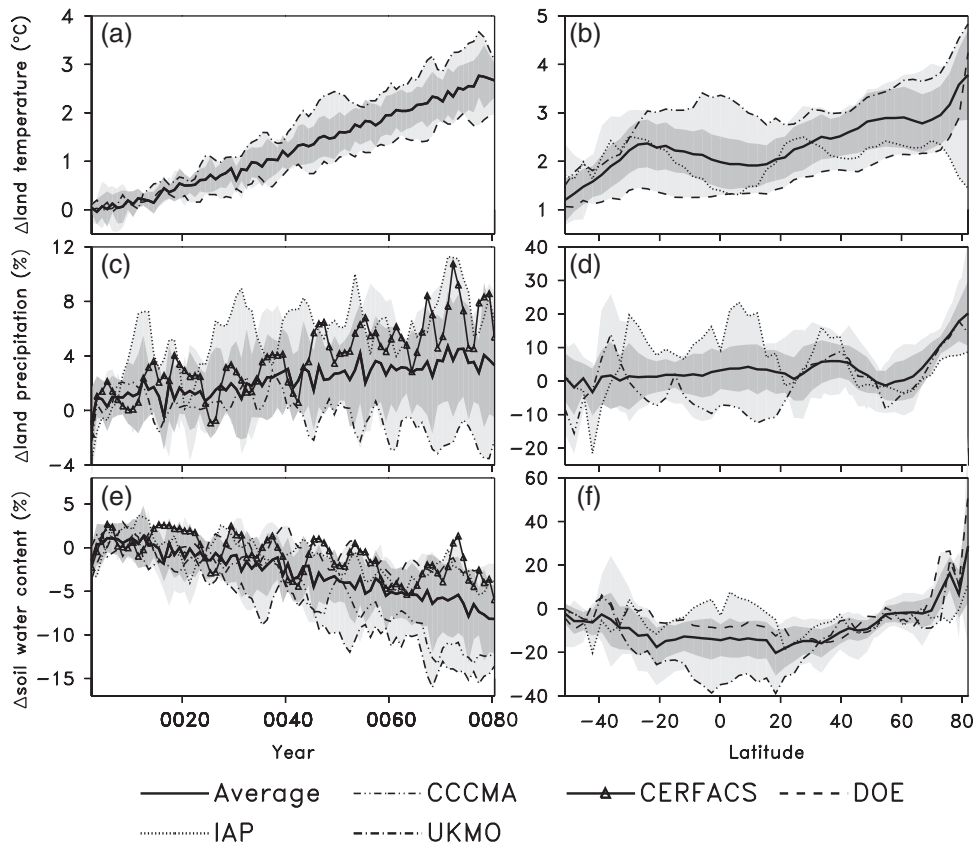


**Fig. 1** The left columns shows the time series of climate forcing used to calculate carbon fluxes: changes of global average land temperature in °C, land precipitation in % and soil water content in % expressed as a difference between FertClim and Fert simulations. The right columns show the latitudinal changes in climate forcing between the last 10 years and the first 10 years of the simulation. The black curve represents the average of all the simulations, the dark shading the two standard error limits, and the light shading the maximum and the minimum envelope.

in the presence of rising  $\text{CO}_2$  enhancing NPP. We found that NEP, under climate change and rising  $\text{CO}_2$ , reaches up to lower values than implied by rising  $\text{CO}_2$  alone. This is quantified by taking the difference between the results of FertClim and Fert simulations, that is herein described using the ‘ $\Delta$ ’ symbol. The ‘between models’ mean value of  $\Delta\text{NEP}$  is of  $-3.7 \text{ Gt C yr}^{-1}$  with a standard deviation of  $2.7 \text{ Gt C yr}^{-1}$ , which corresponds to a relative change  $\Delta\text{NEP}/\text{NEP}$  of  $-27 \pm 20\%$  less uptake in response to climate impact. There is a significant spread in  $\Delta\text{NEP}$  as evidenced in Fig. 2, but this spread is also remarkably parallel to the spread of SWC, suggesting that  $\Delta\text{NEP}$  is primarily sensitive to SWC change (Fig. 1e). To further elucidate the correlation between  $\Delta\text{SWC}$  and  $\Delta\text{NEP}$ , we analyzed how climate change modifies separately the input of carbon to ecosystems by NPP and the output via RH. Globally, NPP is reduced by climate change, with  $\Delta\text{NPP}$  amounting to  $-6.9 \pm 4.0 \text{ Gt C yr}^{-1}$ . This signal is driven by the response of tropical ecosystems that suffer from drought stress (Fig. 3a). The large standard deviation

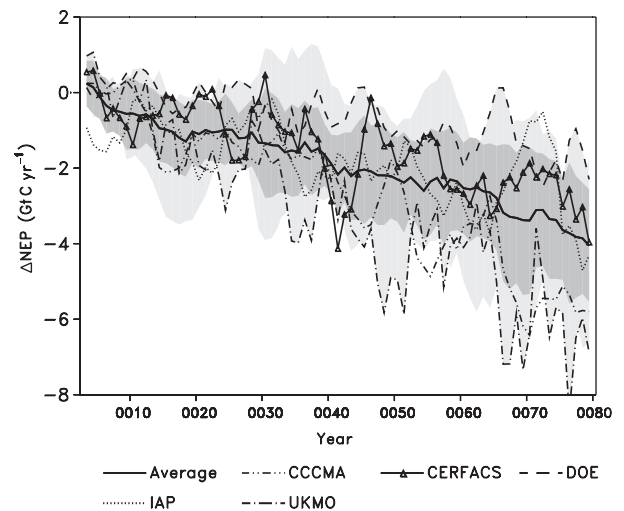


**Fig. 2** Time series of changes in net land uptake (NEP) induced by climate change (in  $\text{Gt C yr}^{-1}$ ) expressed as a difference between FertClim and Fert simulations. Negative values mean that NEP gets reduced under climate change.

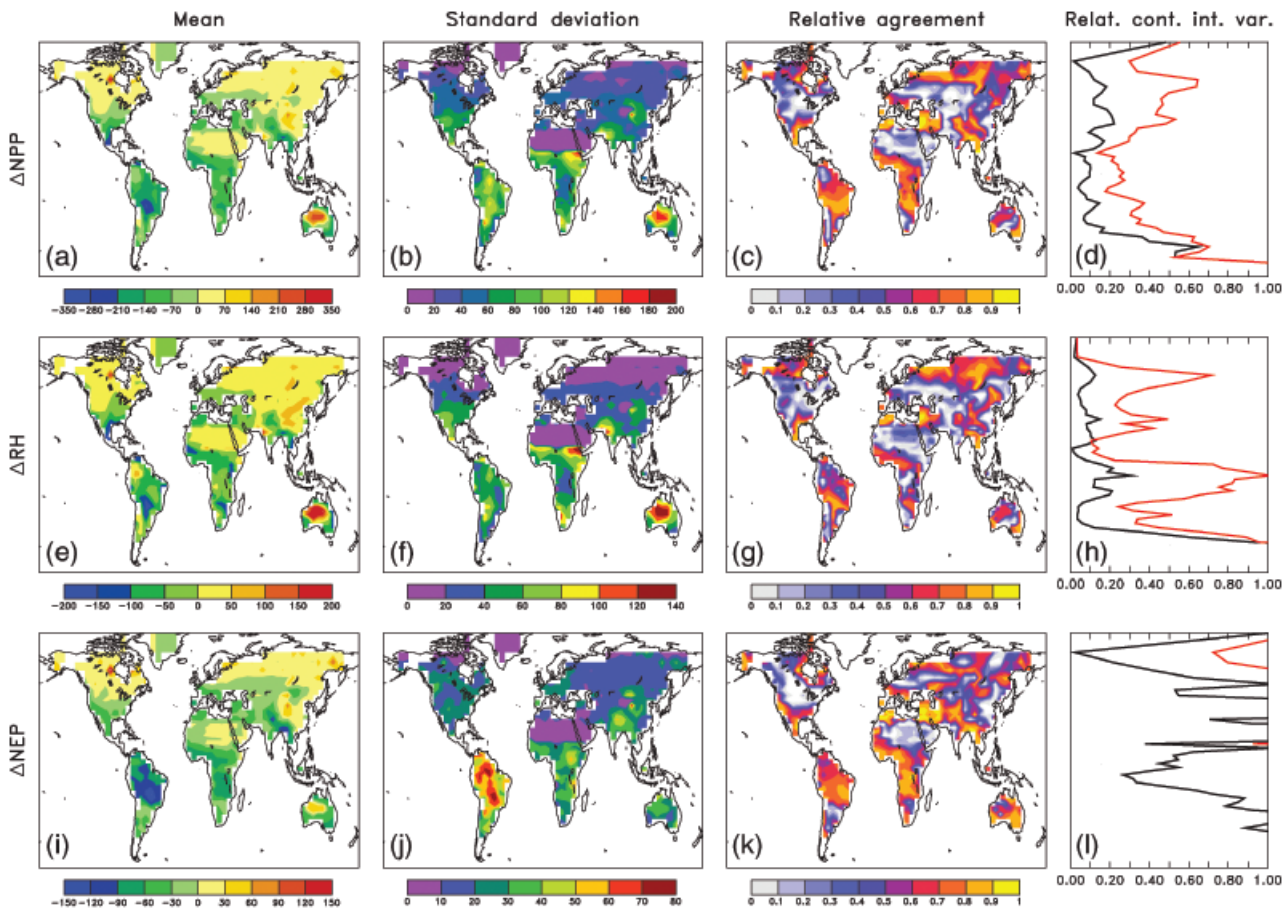


**Fig. 3** Spatial distribution of the mean (first left column) (in  $\text{g C m}^{-2}$ ), standard deviation (second column) (in  $\text{g C m}^{-2}$ ), interexperiment relative agreement ( $F$ ) (third column) and relative contribution of internal variability ( $I$ ) (fourth column) of net primary productivity, heterotrophic respiration and net land uptake changes. In the last column, the dashed line corresponds to the global signal and the solid one to the zonal averaged signal; see text for definitions.

between models (Fig. 3b) is mainly because of various degrees of soils drying in the tropics. Warmer and drier climates induce a pronounced reduction in tropical NPP as illustrated by the UKMO, IPSL and CCCMA results. Unlike in the tropics, at northern latitudes, all models consistently predict an increase in NPP, which in turn results in an increase in NEP (Fig. 3a and i). The reason for this is that rising temperatures act to advance the growing season, which favors additional carbon sequestration in spring (Berthelot *et al.*, 2002). The growing season is typically advanced by 4 days in ECHAM3 or IPSL simulations, and by up to 10 days in UKMO simulation by the end of the simulation. The NEP amplitude thus increases in response to climate change until July but decreases during the second part of the growing season (August and September), as most of climate models simulate temperature greater than optimum temperature for photosynthesis. The average of NEP change during the growing season (April–September) shows an increase for most of the experi-

ences, mostly explained by a greater NEP in FertClim simulation than in the Fert one in the beginning of the growing season.

RH follows the response of NPP to climate, with some lag because of the turnover of carbon (Fig. 3e). Although RH depends directly on temperature via  $Q_{10}$ , we found that the response of respiration to climate change is mostly governed by change in decomposing soil carbon itself reflecting the evolution of NPP. In regions where NPP decreases because of climate change (e.g. the Amazon), RH will also decrease, even if the decomposition rate gets higher.

In summary, despite large spread amongst models, we found that drier and warmer conditions in the tropics act to reduce NPP and thus NEP, and warmer temperatures in the Northern Hemisphere augment NPP and NEP. In the global signal, the tropical reduction is in most cases larger than the Northern Hemisphere increase. In addition, the regions with larger than average NPP, RH and NEP changes also

generally have a larger standard deviation (Fig. 3b, f and j).

#### Agreement and disagreement between modeled land carbon quantities

*Statistical framework.* We now examine how the response of carbon sinks to climate change differs under each future climate simulation. To do so, we applied the statistical tools developed by Räisänen, (2000); Räisänen (2001) to determine similarities and differences between scenario-driven carbon quantities. The method developed by Räisänen (2001) ideally requires an infinitely large population of model runs, which is approximated here by the 14 scenarios. The change in each member of this population can be written as

$$X_{ij} = M + \delta_i + \eta_{ij}, \quad (6)$$

where  $M$  is the mean value for the whole population,  $\delta_i$  a model related deviation and  $\eta_{ij}$  a deviation associated with internal variability in experiment  $ij$ . Index  $i$  corresponds to the number of models used,  $j$  represents the experiments made using the same model but differing in their initial conditions. However, in our case, the sample is composed of a finite numbers of models (14) and only one experiment has been run for each model. In the absence of such ensembles, the two terms  $\delta_i + \eta_{ij}$  also can not be separated directly; we thus used the method developed by Räisänen (2001), which was previously adapted to the CMIP2 experiments.

We obtain an analogous expression for the *squared change* ( $A^2$ ) in any modeled quantity at the end of the simulation: it can be written as the sum of the *mean square value* ( $M^2$ ) of the different scenarios over the last 20 years of integration, and of the *total interexperiment variance* ( $E^2$ ) of all the model runs, so that  $A^2 = M^2 + E^2$ . The total interexperiment variance  $E^2$  in the 14 experiments is further separated into the sum  $E^2 = D^2 + N^2$ , where  $N^2$  refers to a *within model variance* ( $N^2 \equiv \{\eta^2\}$ ) containing the contribution of internal variability (noise), yielding a range of results within each model.  $D^2$  is a *between model variance* ( $D^2 \equiv \{\delta^2\}$ ) associated with the differences implied by distinct climate change scenarios as used to calculate carbon quantities.

The contribution of  $D^2$  and  $N^2$  to the total interexperiment variance must be separated in an indirect way. We estimated the value of the within model variance  $N^2$  after Räisänen (2000) by first separating each 80 years time series into four segments of 20 years duration, second removing a linear trend in each time segment to the difference between FertClim and Fert simulations, third

computing the variance of the residuals to the linear fit within each of the four segments and fourth taking an average of these four estimates of  $N^2$ . We estimated the between model variance  $D^2$  as the difference between  $E^2$  and  $N^2$ .

Useful quantities can be constructed using such statistical decomposition, especially the *Relative Agreement* (called  $F$ ) defined by

$$F = \frac{M^2}{A^2}. \quad (7)$$

The value of  $F$  indicates whether all the 14 experiments have a coherent common signal or not. A value of 1 would mean perfect agreement among the different experiments, and the agreement between models is significant only if  $F \geq 0.5$ . While  $F$  allows us to study if the modeled quantities are in agreement, the disagreement can be divided into contributions of *model differences* (called  $M$ ) and *internal variability* (called  $I$ ), according to

$$\begin{aligned} I &= \frac{N^2}{E^2}, \\ M &= \frac{D^2}{E^2}. \end{aligned} \quad (8)$$

## Results

We first examined the agreement between the different scenarios for the modeled  $\Delta\text{NPP}$ . The interexperiment relative agreement in  $\Delta\text{NPP}$  induced by climate change,  $F_{\Delta\text{NPP}}$  is higher than 0.6 north of  $55^\circ\text{N}$  (Fig. 3c). In this region, increasing temperatures ( $\Delta T$ ) are the main driver of NPP changes (see the section *Spatial patterns in the response of carbon uptake to climate change*), and  $F$  for modeled  $\Delta T$  is above 0.8 (Räisänen, 2001). Two other regions where the modeled  $\Delta\text{NPP}$  shows a common behavior with  $F_{\Delta\text{NPP}} > 0.7$  are the Mediterranean area and the tropics (Fig. 3c), where SWC changes are strongly coherent among the different climate scenarios ( $F_{\Delta\text{SWC}} > 0.7$ ). In those two regions, SWC change is mostly controlled by temperature changes, which are highly coherent, rather than by PPT change.

For high northern latitudes, the Mediterranean regions and the tropics, we found that the total interexperiment variance  $E_{\Delta\text{NPP}}^2$  is mostly attributed to between model errors, rather than to within model errors (Fig. 3d). Over such regions, the contribution of the within model noise to the modeled change in NPP,  $I_{\Delta\text{NPP}}$  does not exceed 0.4 because of small internal variability on the  $\Delta T$  and  $\Delta\text{SWC}$  signals used as an input to force NPP. When the  $\Delta\text{NPP}$  signal is zonally averaged,  $F_{\Delta\text{NPP}}$  increases above 0.8 in the bands  $45\text{--}30^\circ\text{S}$ ,  $20^\circ\text{S}\text{--}40^\circ\text{N}$  and  $>55^\circ\text{N}$ , whereas  $I_{\Delta\text{NPP}}$  drops down to below 0.2 (Fig. 3d). Similar to the response of

climate variables to increased radiative forcing (Räsänen, 2001), the response of NPP to various climate scenarios, as assessed in our case by a unique terrestrial carbon model, becomes more coherent when spatial averaging is applied to the model fields. However, in some areas, spatial averaging does not improve  $F_{\Delta\text{NPP}}$  because it increases the contribution of the 'between-model' variance  $D^2$  to the squared change  $A^2$  (in particular in the band 50–45°S).

Second, we inspected the common behavior of change in RH from  $F_{\Delta\text{RH}}$ . Wherever  $\Delta\text{NPP}$  is coherent,  $\Delta\text{RH}$  is also coherent (Fig. 3g). This not so surprising since changes in RH primarily reflect changes in NPP, with some time lag because of the turnover of carbon in ecosystems (Berthelot *et al.*, 2002). There is an exception to this rule for the forest ecosystem around the equator (10°S to 0°), where  $F_{\Delta\text{RH}}$  is lower than 0.5, whereas  $F_{\Delta\text{NPP}}$  is higher than 0.6. Over that particular region, the disagreement in  $\Delta\text{RH}$  between the different climate scenarios is because of a proportionally larger contribution of the within model noise variability, with  $I_{\Delta\text{RH}} > 0.8$  (Fig. 3h). The value of  $\Delta\text{RH}$  for a given climate scenario reflects how a change in climate modifies the product of soil carbon pools by their decomposition rates (the latter being dependant on temperature and soil moisture). The fact that  $\Delta\text{RH}$  is less coherent than  $\Delta\text{NPP}$  around the equator can thus be explained either by a low  $F$  in the soil carbon pools change or by a low  $F$  in the decomposition rates change, or a combination of both. We have calculated a  $F > 0.7$  for the soil carbon pools change and  $F < 0.4$  for the decomposition rates change showing that the disagreement in  $\Delta\text{RH}$  at the equator is mostly because of the differences in decomposition rates changes variability (temperature, soil moisture) rather than to differences in decomposing soil pools. When averaging zonally  $\Delta\text{RH}$ , the  $F$  increases and becomes close to  $F_{\Delta\text{NPP}}$  excepted around the equator.

Third, we looked at the common behavior in  $\Delta\text{NEP}$ . Mapping  $F_{\Delta\text{NEP}}$  (Fig. 3k) shows a geographic distribution that is quite parallel to the ones of  $F_{\Delta\text{NPP}}$  (Fig. 3c). However, unlike for NPP, the total variance of  $\Delta\text{NEP}$  is mostly attributed to the 'within model' noise (Fig. 3l) rather than to the 'between model' spread (Fig. 2). This is because, as in Räsänen, (2001), in the absence of an ensemble of climate simulations for any given climate model, we approximate the 'within model' noise  $I_{\Delta\text{NEP}}$  by the signal of interannual variability in  $\Delta\text{NEP}$ . The interannual variability of  $\Delta\text{NEP}$  reflects the ones of  $\Delta\text{NPP}$  and the one of  $\Delta\text{RH}$ , which is governed by the effect of climate interannual variations on decomposition rates of soil organic matter. Therefore,  $I_{\Delta\text{NEP}}$  includes both noise in  $\Delta\text{NPP}$ , which generates noise on the size of decomposing soil carbon pools, and noise

in the specific rates of decomposition. This is likely not to be a specific feature of the SLAVE carbon model, since nearly all studies of today's interannual variability of NEP (Kindermann *et al.*, 1996; Jones *et al.*, 1998; Tian *et al.*, 1998; Gerard *et al.*, 1999; Botta *et al.*, 2000) have demonstrated that interannual variations in NPP are equally as important as those in RH in determining the fluctuations of NEP.

### Sensitivity of the results to the carbon model parameters

How NEP changes in response to climate change obviously depends on the land carbon cycle model that is employed. Would the conclusions of the former section be strongly different if modeled NPP was more or less sensitive to CO<sub>2</sub> increase, or RH more or less sensitive to soil warming and drying? We tested the sensitivity of  $\Delta\text{NEP}$  to varying pairs of ( $\beta_0$ ,  $Q_{10}$ ) (Eqns (2)–(4)) both for a warm climate model scenario (IPSL) and for a cold scenario (DOE).

We varied the value of  $\beta_0$  in Eqn (2) between 0.2 and 1 around the control setting of 0.65, which best matches the historical CO<sub>2</sub> curve (Friedlingstein *et al.*, 1995).

We also varied the dependency of soil respiration on temperature,  $Q_{10}$ , between 1 and 3 around its standard value of 2. For each ( $\beta_0$ ,  $Q_{10}$ ) pair, we recomputed an initial carbon state for SLAVE, and then a Fert and FertClim simulation, using DOE and IPSL changing climate scenarios, to estimate the impact of climate change on NEP.

When  $\beta_0$  increases,  $\Delta\text{NEP}/\text{NEP}$  tends to decrease as the increase in NEP because of rising CO<sub>2</sub> is larger than the increase in the climate change impact on NEP. It means that for a very strong fertilization effect, the impact of climate change in lowering the uptake of CO<sub>2</sub> becomes secondary (Table 3). Another extreme is the case of no fertilization at all ( $\beta_0 = 0$ ), in which rising CO<sub>2</sub> generates no additional carbon uptake, whereas climate change would act to turn the land biosphere into a source of carbon.

When  $Q_{10}$  increases,  $\Delta\text{NEP}/\text{NEP}$  tends to increase. This is because higher  $Q_{10}$  accelerates the oxidation of soil carbon, and hence RH tracks more quickly increasing NPP, inducing *in fine* a smaller net uptake of carbon (Table 3).

In the two experiences DOE-SLAVE and LMD-SLAVE,  $\Delta\text{NEP}$  responds qualitatively in the same way to changing  $\beta_0$  and  $Q_{10}$ : If  $\beta_0$  increases or  $Q_{10}$  increases,  $\Delta\text{NEP}$  increases for both scenarios. This suggests that the 'transfer function' between 'input climate scenarios' and 'output'  $\Delta\text{NEP}$  given in Fig. 2 could be conserved throughout a large range of varying  $\beta_0$  and  $Q_{10}$ . Hence, the conclusions of this section on how different climate



scenarios qualitatively resulted in different  $\Delta\text{NEP}$  are likely to hold true for different settings of the parameters of the SLAVE terrestrial carbon model.

However, if one desires accurate quantification of  $\Delta\text{NEP}$ , then varying the biospheric model's parameters turns out to be equally as important as going from one climate scenario to another. The difference between  $\Delta\text{NEP}/\text{NEP}$  modeled under a cold climate scenario and under a warm scenario reaches up to 30% and from 12% to 44% if we change biopsheric parameters (Table 3).

### Relationship between the impact of climate change on carbon fluxes and the sensitivity of climate to changes in radiative forcing

The sensitivity of the terrestrial carbon uptake to increasing temperature can be expressed as  $\gamma$ , the ratio

**Table 3** Relative change in NEP induced by climate change for different settings of two key parameters in the SLAVE model: the biotic growth factor  $\beta$  and the temperature dependency of soil respiration  $Q_{10}$

$\Delta\text{NEP}/\text{NEP}$	$\beta$			$Q_{10}$		
	0.2	0.65	1	1	2	3
DOE	-30%	-15%	-11%	-8%	-15%	-20%
IPSL	-87%	-43%	-33%	-35%	-43%	-50%

Two different GCMs climate forcings are examined: DOE and IPSL.

NEP, net land uptake; GCM, general circulation model.

**Table 4** Global climate sensitivity of the OAGCM to  $\text{CO}_2$  increase ( $\alpha = \Delta T / \Delta\text{CO}_2$ ) and global carbon sensitivity of SLAVE to climate change ( $\gamma = \Delta\text{NEP} / \Delta T$ )

OAGCM	$\gamma$ ( $\text{GtC } ^\circ\text{C}^{-1}$ )	$\alpha$ ( $^\circ\text{C ppm}^{-1}$ )
BMRC	-73.9	$5.5 \times 10^{-3}$
CCCMA	-55.6	$6.7 \times 10^{-3}$
CCSR	-64.8	$5.7 \times 10^{-3}$
CERFACS	-40.7	$5.7 \times 10^{-3}$
CSIRO	-33.2	$7.0 \times 10^{-3}$
DOE	-22.0	$4.6 \times 10^{-3}$
ECHAM3	-46.5	$5.5 \times 10^{-3}$
GFDL	-40.2	$7.5 \times 10^{-3}$
GISS	-43.9	$5.1 \times 10^{-3}$
IAP	-61.7	$5.8 \times 10^{-3}$
IPSL	-68.9	$7.0 \times 10^{-3}$
MRI	-6.7	$5.6 \times 10^{-3}$
NCAR	-32.9	$5.1 \times 10^{-3}$
UKMO	-63.0	$7.2 \times 10^{-3}$
Experiment average	$-46.7 \pm 19.2$	$(6.0 \pm 0.9) \times 10^{-3}$

OAGCM, ocean-atmosphere general circulation model.

of cumulated  $\Delta\text{NEP}$  to  $\Delta T$ . A larger 'carbon sensitivity'  $\gamma$  in a coupled carbon-climate simulation such as the one performed by Cox *et al.* (2000) would translate into strong climate-carbon cycle positive feedbacks with faster increase in atmospheric  $\text{CO}_2$  and more pronounced temperature rise. When considering  $\Delta\text{NEP}$  and  $\Delta T$  averaged over the last 20 years of each simulation, the most negative  $\gamma$  values correspond to the BMRC, CCSR, IPSL and UKMO models (Table 4). The interexperiment average value of  $\gamma$  is of  $-47 \pm 19 \text{ GtC yr}^{-1} ^\circ\text{C}^{-1}$  (Table 4) and it is mainly explained by the behavior of tropical biomes, over which the NEP reduction is important because of soil drying.

We correlated in each simulation the 'carbon sensitivity' with the OAGCM climate sensitivity  $\alpha$ , expressed as the ratio between land temperature increase,  $\Delta T$ , and atmospheric  $\text{CO}_2$  increase,  $\Delta\text{CO}_2$ . A large value of means that for a given increase in  $\text{CO}_2$  radiative forcing, water vapor, clouds and other physical feedbacks in the climate system act to strongly amplify the  $\text{CO}_2$  induced change in temperature. We can see in Fig. 4 that the simulations with the highest  $\alpha$  (UKMO, IPSL) also have a more negative  $\gamma$  in the tropics. In the latitude band  $25^\circ\text{S}$ – $25^\circ\text{N}$ , the correlation coefficient between  $\alpha$  and  $\gamma$  reaches up to  $-0.6$  (with a 98% significant level as calculated using the bilateral student test). In other words, the more sensitive a given GCM climate to increasing  $\text{CO}_2$ , the more important the reduction of terrestrial carbon uptake per  $1^\circ\text{C}$  warming in the tropics. This result is not directly intuitive, but it suggests that the mechanisms that act in the climate

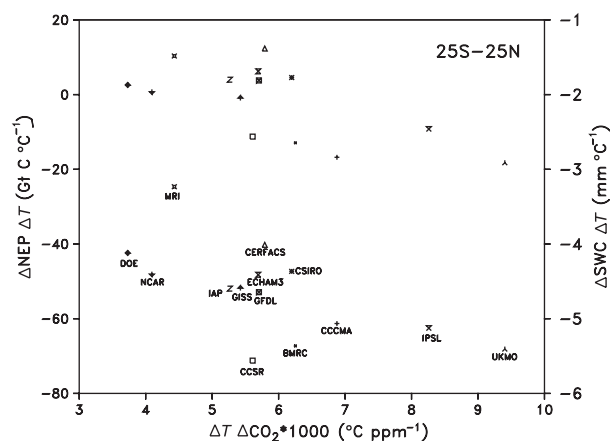


**Fig. 4** Subscribed symbols: carbon sensitivity defined as the change in net land uptake normalized by degree warming as a function of climate sensitivity defined as the change in temperature per ppm of additional atmospheric  $\text{CO}_2$ . Other symbols: sensitivity of soil water content to temperature as a function of climate sensitivity. All variables are averaged over tropical lands in the band  $25^\circ\text{S}$ – $25^\circ\text{N}$ .

system to amplify the radiative forcing of CO<sub>2</sub> are also causing a reduction in the carbon uptake by tropical plants. We searched for a mechanism or a chain of mechanisms, which correlate the climate sensitivity with the carbon sensitivity. Since tropical NEP in SLAVE is mainly controlled by SWC, the correlation between  $\gamma$  and the sensitivity of SWC change to increasing temperature ( $\Delta\text{SWC}/\Delta T$ ) is high (0.9). Thus, we regressed  $\Delta\text{SWC}/\Delta T$  as a function of  $\alpha$  over the tropics (Fig. 4), and obtained a correlation of 0.7 (98% significance). A possible explanation could be that a reduction in SWC increases the resistance for surface evaporation, and thereby reduces the latent heat flux. To balance approximately the same solar net radiation, this would translate into an increase in surface temperature and therefore of sensible heat flux and long wave radiation. Another possible explanation is that the more sensitive OAGCM have initial drier land surface states and are therefore less able to dissipate additional energy as latent heat.

In coupled carbon climate simulations, the models with large climate sensitivities to CO<sub>2</sub> might thus be those with the largest soil drying, and therefore those with the largest reduction of carbon uptake and *in fine* the largest climate-carbon positive feedbacks. Interestingly, the only two GCMs that have performed climate carbon coupled simulations, IPSL (Dufresne *et al.*, 2002) and UKMO (Cox *et al.*, 2000), show precisely the highest values and large  $\gamma$  (Fig. 4).

## Conclusion

We used 14 CMIP2 OAGCM climate simulations to force the biosphere model SLAVE in order to estimate how the range in future climate prediction translates into terrestrial carbon storage. All the experiments show that climate change acts to globally reduce the terrestrial carbon uptake. However, the regional distribution of NEP reduction can be very different according to the OAGCM used. We use a variance decomposition method to quantify the interexperiment agreement and to separate the uncertainty because of differences between models because of model internal variability. Agreement between modeled land temperature changes is very good, but this is not the case for PPT and SWC changes. We find that there is a good model agreement on the responses of tropical, Mediterranean and high northern latitudes NPP and NEP to climate change. For example, the NEP reduction in the tropics is a pattern present in the majority of the 14 simulations. In those regions, the residual disagreement in carbon quantities is mostly explained by scenario differences when we consider NPP, RH and pools

changes, but, on the contrary, it is rather explained by high internal variability for NEP change.

As internal variability may hide the climate change impact on NEP, we thus have to increase the averaging period to improve the estimation of NEP change. An average over a decade may be necessary to detect climate change impact on NEP signal as a shorter averaging period would have kept a large internal variability.

The land biospheric carbon pool reduction because of climate change, varies from 30 GtC for the less sensitive experiment (MRI, which shows low climate sensitivity to CO<sub>2</sub> increase,  $\alpha$ , and the lowest sensitivity of carbon storage to changing climate,  $\gamma$ ) to 240 GtC for the most sensitive models (IPSL and UKMO, largest  $\alpha$  and large  $\gamma$ ) by the end of the simulation. We also performed a sensitivity study on the carbon cycle response to climate change by varying the values of  $Q_{10}$  and  $\beta_0$ , and found that this leads to an uncertainty in carbon storage changes that is as important as the one induced by the spread in climate change scenarios. Consequently, the systematic forcing of a carbon cycle model using a range of climate scenarios should be clearly extended to carbon cycle models with other parameterizations.

Finally, the use of several climate scenarios allows us to correlate the sensitivity of carbon storage to climate change with climate sensitivity to increasing CO<sub>2</sub> in the tropical band. We find that when SLAVE is forced by the GCM with the largest climate sensitivity, it also simulates a stronger reduction of NEP per 1 °C of warming. A possible mechanism to explain such a relation is the following: the reduction of NEP as mainly driven by a reduction in SWC would induce a reduction of latent heat flux. This could lead to an increase in surface temperature, sensible heat flux and long-wave radiation. Another explanation could be the drier initial state of land surface that goes against dissipation of additional latent heat flux.

It is worth noting as a conclusion that the only two climate models that performed climate-carbon simulations (Cox *et al.*, 2000; Dufresne *et al.*, 2002) are the ones with the largest  $\alpha$  and large  $\gamma$ . We may thus anticipate that the positive climate-carbon feedback could then be lower when coupled simulation will become available from other climate models.

## Acknowledgements

We are grateful to the participants of the Coupled Model Intercomparison Project 2 to have provided us with their model output. We thank H. Le Treut for helpful discussions at an earlier stage of this manuscript. This work was partly supported by the French PNEDC Program.

## References

- Barthelet P, Terray L, Valcke S (1998) Transient CO<sub>2</sub> experiment using the ARPEGE/OPAICE nonflux corrected coupled model. *Geophysical Research Letters*, **25**, 2277–2280.
- Berthelot M, Friedlingstein P, Ciais P *et al.* (2002) Global response of the terrestrial biosphere to CO<sub>2</sub> and climate change using a coupled climate-carbon cycle model. *Global Biogeochemical Cycles*, **16**, 1084–1100.
- Bishop JB, Rossow WB (1991) Spatial and temporal variability of global surface solar irradiance. *Journal of Geophysical Research*, **96**, 16839–16858.
- Boer GJ, Flato G, Ramsden D (2000) A transient climate change simulation with greenhouse gas and aerosol forcing: projected climate to the twenty-first century. *Climate Dynamics*, **16**, 427–450.
- Botta A, Viovy N, Ciais P *et al.* (2000) A global prognostic scheme of leaf onset using satellite data. *Global Change Biology*, **6**, 709–725.
- Boville BA, Gent PR (1998) The NCAR climate system model, version one. *Journal of Climate*, **11**, 1115–1130.
- Cao M, Woodward FI (1998) Dynamic responses of terrestrial ecosystem carbon cycling to global climate change. *Nature*, **393**, 249–252.
- Colman RA (2001) On the vertical extent of atmospheric feedbacks. *Climate Dynamics*, **17**, 391–405.
- Covey C, AchutaRao KM, Cubasch U *et al.* (2003) An overview of results from the coupled model intercomparison project. *Global and Planetary Change*, **37**, 103–133.
- Cox PM, Betts RA, Jones CD *et al.* (2000) Acceleration of global warming due to carbon-cycle feedbacks in a coupled climate model. *Nature*, **408**, 184–187.
- Cramer W, Bondeau A, Woodward FI *et al.* (2001) Global response of terrestrial ecosystem structure and function to CO<sub>2</sub> and climate change: results from six dynamic global vegetation models. *Global Change Biology*, **7**, 357–373.
- Cubasch U, Voss R, Hegerl GC *et al.* (1997) Simulation of the influence of solar radiation variations on the global climate with an ocean-atmosphere general circulation model. *Climate Dynamics*, **13**, 757–767.
- Dai A, Fung IY, DelGenio AD (1997) Surface observed global land precipitation variations during 1900–88. *Journal of Climate*, **10**, 2943–2962.
- DeLucia EH, Hamilton JG, Naidu SL *et al.* (1999) Net primary Production of a forest ecosystem with experimental CO<sub>2</sub> enrichment. *Science*, **284**, 1177–1179.
- Delworth TL, Knutson TR (2000) Simulation of early 20th century global warming. *Science*, **287**, 2246–2250.
- Dufresne JL, Friedlingstein P, Berthelot M *et al.* (2002) On the magnitude of positive feedback between future climate change and the carbon cycle. *Geophysical Research Letter*, **29**.
- Emori S, Nozawa T, Abe-Ouchi A *et al.* (1999) Coupled ocean-atmosphere model experiments of future climate change with an explicit representation of sulfate aerosol scattering. *Journal of Meteorological Society of Japan*, **77**, 1299–1307.
- Flato GM, Boer GJ, Lee WG *et al.* (2000) The Canadian centre for climate modelling and analysis global coupled model and its climate. *Climate Dynamics*, **16**, 451–467.
- Friedlingstein P, Fung I, Holland E *et al.* (1995) On the contribution of CO<sub>2</sub> fertilization to the missing biospheric sink. *Global Biogeochemical Cycles*, **9**, 541–556.
- Friedlingstein P, Joel G, Field CB *et al.* (1999) Toward an allocation scheme for global terrestrial carbon models. *Global Change Biology*, **5**, 755–770.
- Gerard JC, Nemry B, Francois LM *et al.* (1999) The interannual change of atmospheric CO<sub>2</sub>: contribution of subtropical ecosystems? *Geophysical Research Letters*, **26**, 243–246.
- Gifford RM (1992) Interaction of carbon dioxide with growth-limiting environmental factors in vegetation productivity: implications for the global carbon cycle. *Advances in Bioclimatology*, **1**, 24–58.
- Gordon C, Cooper C, Senior CA *et al.* (2000) The simulation of SST, sea ice extents and ocean heat transports in a version of the Hadley Centre coupled model without flux adjustments. *Climate Dynamics*, **16**, 147–168.
- Gordon HB, O'farrell SP (1997) Transient climate change in the CSIRO coupled model with dynamic sea ice. *Monthly Weather Review*, **125**, 875–907.
- Hansen J, Ruedy R, Glascoe J *et al.* (1999) GISS analysis of surface temperature change. *Journal of Geophysical Research*, **104**, 30997–31022.
- Hirst AC, O'farrell SP, Gordon HB (2000) Comparison of a coupled ocean-atmosphere model with and without oceanic eddy-induced advection. 1. Ocean spin-up and control integrations. *Journal of Climate*, **13**, 139–163.
- IPCC (2001) *Climate Change 2001: The Scientific Basis – Contribution of Working Group I to the IPCC Third Assessment Report*, R. Watson, J. Houghton, D. Yihui, New York.
- Jones TH, Thompson LJ, Lawton JH *et al.* (1998) Impacts of rising atmospheric carbon dioxide on model terrestrial ecosystems. *Science*, **280**, 441–443.
- Khodri M, Leclainche Y, Ramstein G *et al.* (2001) Simulating the amplification of orbital forcing by ocean feedbacks in the last glaciation. *Nature*, **410**, 570–574.
- Kindermann J, Wurth G, Kohlmaier GH *et al.* (1996) Interannual variation of carbon exchange fluxes in terrestrial ecosystems. *Global Biogeochemical Cycles*, **10**, 737–755.
- Los SO, Justice CO, Tucker CJ (1994) A global 1° by 1° NDVI data set for climate studies derived from the GIMMS continental NDVI data. *International Journal of Remote Sensing*, **15**, 3493–3518.
- Matthews E (1983) Global vegetation and land use: new high resolution data bases for climate studies. *Journal of Climate and Applied Meteorology*, **22**, 474–487.
- Meehl GA, Boer GJ, Covey C *et al.* (2000) The coupled model intercomparison project (CMIP). *Bulletin of American Meteorological Society*, **81**, 313–318.
- Parton WJ, Scurlock JMO, Ojima DS *et al.* (1993) Observations and modeling of biomass and soil organic matter dynamics for the grassland biome worldwide. *Global Biogeochemical Cycles*, **7**, 785–809.
- Potter CS, Randerson JT, Field CB *et al.* (1993) Terrestrial ecosystem production: a process model based on global satellite and surface data. *Global Biogeochemical Cycles*, **7**, 811–841.
- Power SB, Tseitkin F, Colman RA *et al.* (1998) *A Coupled General Circulation Model for Seasonal Prediction and Climate Change*

- Research*. BMRC Research Report, Bureau of Meteorology, Melbourne, Australia.
- Räisänen J (2001) CO<sub>2</sub> induced climate change in CMIP experiments: quantification of agreement and role of internal variability. *Journal of Climate*, **14**, 2088–2104.
- Räisänen J (2000) *CO<sub>2</sub>-Induced Climate Change in Northern Europe: Comparison of 12 CMIP2 Experiments*. Reports Meteorology and Climatology, Swedish Meteorological and Hydrological Institute, Norrköping, Sweden.
- Russell GL, Miller JR, Rind D (1995) A coupled atmosphere-ocean model for transient climate change studies. *Atmosphere-Ocean*, **33**, 683–730.
- Russell GL, Rind D (1999) Response to CO<sub>2</sub> transient increase in the GISS coupled model: regional coolings in a warming climate. *Journal of Climate*, **12**, 531–539.
- Sellers PJ, Randall DA, Collatz GJ *et al.* (1996) A revised land-surface parametrization (Sib2) for atmospheric GCMs, I, Model formulation. *Journal of Climate*, **9**, 676–705.
- Thornthwaite CW (1948) An approach toward a rational classification of climate. *Geographical Review*, **38**, 55–89.
- Thornthwaite CW, Mather JR (1957) Instructions and tables for computing potential evapotranspiration and the water balance. *Publications in Climatology*, **10**, 181–311.
- Tian HQ, Melillo JM, Kicklighter DW *et al.* (1998) Effect of interannual climate variability on carbon storage in Amazonian ecosystems. *Nature*, **396**, 664–667.
- Tokioka T, Noda A, Kitoh A *et al.* (1996) *A transient CO<sub>2</sub> experiment with the MRI CGCM: annual mean response*. CGER's Supercomputer Monograph Report. Center for Global Environmental Research, National Institute for Environmental Studies, Environment Agency of Japan, Ibaraki, Japan.
- Voss R, Sausen R, Cubasch U (1998) Periodically synchronously coupled integrations with the atmosphere-ocean general circulation model ECHAM3/LSG. *Climate Dynamics*, **14**, 249–266.
- Washington WM, Weatherly JM, Meehl GA *et al.* (2000) Parallel climate model (PCM) control and transient simulations. *Climate Dynamics*, **16**, 755–774.
- Wu G-X, Zhang X-H, Liu H *et al.* (1997) Global ocean-atmosphere-land system model of LASG (GOALS/LASG) and its performance in simulation study. *Quarterly Journal of Applied Meteorology*, **8**, 15–28.
- Wullschleger SD, Post WM, King AW (1995) On the potential for a CO<sub>2</sub> fertilization effect in forests: estimates of the biotic growth factor based on 58 controlled-exposure studies. In: *Biotic Feedbacks in the Global Climatic System. Will the Warming Feed the Warming?* (eds Woodwell GM, Mackenzie FT), Oxford University Press, New York pp. 85–107.
- Zhang X-H, Shi G-Y, Liu H *et al.* (2000) *IAP Global Atmosphere-Land System Model*. Science Press, Beijing, China.